https://doi.org/10.5194/egusphere-2023-534
Preprint. Discussion started: 23 March 2023
© Author(s) 2023. CC BY 4.0 License.

The intrinsic relationship between cyclones, anticyclones, and Rossby Wave Breakings in the North-Atlantic

Talia Tamarin-Brodsky[1] and Nili Harnik[1]

[1]Department of Geophysics, Tel-Aviv University, Tel-Aviv, Israel

Correspondence: Talia Tamarin-Brodsky (taliatamarin@gmail.com)

Abstract. Rossby wave breaking events describe the last stage in the life-cycle of baroclinic atmospheric disturbances. These breaking events can strongly influence the large-scale circulation, and are also related to weather extremes such as heat waves, blockings, and extreme precipitation events. Nonetheless, a complete understanding of the synoptic-scale dynamics involved with wave breaking events is still absent. Here we highlight the fundamental relation between low-level weather systems and upper-level wave breaking events in the North Atlantic region, by combining a storm-tracking technique together with a wave breaking detection algorithm. We show that Anticyclonic Wave Breaking (AWB) events are associated with a strong upper-level ridge and a low-level anticyclone to its east, which are both located in the anticyclonic side of the jet. During the breaking, a strong cyclone is often found to the north-northwest of the anticyclone, while a weaker one is often found to its south-southeast. Time evolution composites centered around anticyclones during AWB show that as the downstream trough wraps anticyclonically to the east and south of the ridge, the upper-level jet weakens to the south, hence the upper-level jet becomes more split into an upstream poleward tilted jet, and a downstream zonal jet. In addition, the Sea Level Pressure (SLP) anomalies rotate in an anticyclonic manner relative to each other, such that the initially zonally oriented low-high SLP anomaly dipole become meridionally oriented by the end of the life-cycle (low-above-high). On the contrary, Cyclonic Wave Breaking (CWB) events are associated with a strong upper-level trough and a low-level cyclone to its east, which are both located in the cyclonic side of the jet. An additional anticyclone is often found to the northeast of the cyclone. Time evolution composites centered around cyclones during CWB show that as the downstream ridge wraps cyclonically to the east and north of the trough, the zonal and more southward shifted upper-level jet weakens further to the north. A relative cyclonic rotation is observed at low-levels, such that a high-above-low SLP anomaly dipole is found by the end of the life-cycle. A simple kinematic interpretation is suggested for the poleward and equatorward shifted jets associated with AWB and CWB events, respectively. Anomalous life-cycles of anticyclones during CWB events and cyclones during AWB events are also discussed.

1 Introduction

The midlatitude atmospheric circulation is characterized by the continuous passage of propagating synoptic-scale weather systems, which play an important role in the meridional redistribution of momentum, moisture, and heat flux. These anomalous cyclonic and anticyclonic circulations grow via baroclinic instability, as a result of Earth's rotation and the equator-to-pole temperature difference. The waves tend to follow a typical Rossby wave life-cycle, which involves a linear baroclinic growth

https://doi.org/10.5194/egusphere-2023-534
Preprint. Discussion started: 23 March 2023
© Author(s) 2023. CC BY 4.0 License.

stage (Charney, 1947; Eady, 1949) followed by a nonlinear barotropic decay (Simmons and Hoskins, 1978; Davies et al., 1991). During the decay stage, Rossby wave breaking (RWB) occurs, formally defined as a large-scale and irreversible overturning of the potential vorticity (PV) contours on isentropic surfaces (McIntyre and Palmer, 1983). This overturning results in an inversion of the meridional PV gradient, which is often used as a definition of RWB in automated detection algorithms. The PV mixing that occurs in the wave breaking region, and the associated anomalous momentum fluxes, can result in an acceleration/deceleration or meridional shifts of the upper-level jet. In addition, these breaking events were linked to extreme weather events (Martius and Rivière, 2016), such as extreme precipitation (Moore et al., 2019; de Vries, 2021), explosive cyclogenesis (Hanley and Caballero, 2012; Gomara et al., 2014), and tropical cyclone activity (Zhang et al., 2017).

There are two main types of wave breaking, with a very distinct upper-air behaviour, occurring at the end of the baroclinic wave life-cycles (Simmons and Hoskins, 1978; Thorncroft et al., 1993). The first type is dominated by an Anticyclonic Wave Breaking (AWB) (e.g., Fig.1a), and is characterized by a southwest-northeast (SW-NE) tilt of the PV contours. The second type involves Cyclonic Wave Breaking (CWB),(e.g., Fig.1b) and is characterized by a southeast-northwest (SE-NW) tilt of the PV contours. Previous studies have further distinguished between 'equatorward breaking' and 'poleward breaking' cases (e.g., see Fig.1 in Tyrlis and Hoskins (2008) or Fig.1 in Gabriel and Peters (2008) for a schematic illustration). The equatorward breaking cases involve an equatorward extrusion of high-PV air, and were coined LC1 and LC2 by Thorncroft et al. (1993). In LC2, wave breaking occurs on the poleward side of the jet and is therefore associated with CWB, since the ambient cyclonic shear enhances any equatorward extrusion of high-PV (and therefore cyclonic in nature) air. This leads to the development of wide and strong troughs, and prevents the building of strong ridges. However, in LC1, wave breaking occurs equatorward of the jet and is associated with AWB, since the ambient anticyclonic shear suppresses any equatorward extrusions of high-PV air, leading to thinning troughs and possibly to the development of a weak cutoff low (Thorncroft et al., 1993).

The importance of the two poleward breaking cases (P1 and P2), which involve a poleward extrusion of low-PV air, was introduced by Peters and Waugh (1996). In P2, wave breaking occurs on the equatorward side of the jet and is therefore associated with AWB, since the anticyclonic circulation associated with any poleward extrusion of low-PV air is enhanced by the ambient anticyclonic shear. This results in strong blocking-like ridge that tends to develop equatorward of the jet. In P1, the wave breaking occurs poleward of the jet and is therefore associated with CWB, since the ambient cyclonic shear suppresses any poleward extrusion of low-PV air, leading to thinning ridges and often to the development of a weak cutoff ridge (Peters and Waugh, 1996). Hence, P2 and LC1 are dominated by AWB, while P1 and LC2 are dominated by CWB. In all four cases, a reversal in the upper-level meridional PV gradient is observed, but the overturning of the PV contours is weaker in cases P1 and LC1. Most traditional RWB-detection algorithms that rely on the reversal of PV contours only distinguish between AWB and CWB events, and in practice mostly detect the P2 and LC2 types. This is often not acknowledged in studies, where the more familiar LC1 and LC2 life-cycle terminology is used instead. A further investigation of each one of the four breaking types was performed in several studies (e.g., Peters and Waugh, 1996; Tyrlis and Hoskins, 2008; Gabriel and Peters, 2008). Here we use the RWB detection algorithm developed by Strong and Magnusdottir (2008), which can detect both poleward and equatorward breaking events. We configure it to detect the equatorward breaking cases, but our results are qualitatively similar if poleward breaking cases are analyzed instead (see Section 22.2 for more details).

https://doi.org/10.5194/egusphere-2023-534
Preprint. Discussion started: 23 March 2023
© Author(s) 2023. CC BY 4.0 License.

Past studies have shown, in idealized baroclinic life-cycle experiments, that the sense in which the wave breaking occurs (AWB or CWB) can be controlled by changing either the initial meridional shear of the background zonal jet (Simmons and Hoskins, 1978; Davies et al., 1991; Thorncroft et al., 1993; Peters and Waugh, 1996; Hartmann and Zuercher, 1998; Hartmann, 2000; Shapiro et al., 1999), the initial zonal wavenumber of the perturbation (Hartmann and Zuercher, 1998; Orlanski, 2003; Wittman et al., 2007), or the strength of the cyclonic and anticyclonic vortices achieved by adding external forcing or by adding moisture (Orlanski, 2003). The type of breaking can significantly modify the low-frequency atmospheric circulation, and therefore influence the jet variability. In general, during AWBs eddy momentum fluxes are mostly poleward, and the zonal flow is therefore accelerated (decelerated) poleward (equatorward) of the breaking, leading to a poleward shift of the jet. On the contrary, during CWBs momentum fluxes are mainly equatorward, and thus accelerate (decelerate) the zonal flow equatorward (poleward) of the breaking, leading to an equatorward shift of the jet (Simmons and Hoskins, 1978; Thorncroft et al., 1993). Similarily, Orlanski (2003) suggested that when anticyclonic circulations are dominant, the eddy vorticity flux $v'q'$ is positive (negative) poleward (equatorward) of the breaking, which acts to accelerate (decelerate) the zonal flow poleward (equatorward) of the breaking through $\frac{\partial \overline{U}}{\partial t} \sim \overline{v'q'}$, and vice versa for the case where cyclonic circulations are dominant (see Fig. 9 in Orlanski, 2003).

The interaction between the shorter-timescale RWB and the lower-frequency background flow is two-way. On the one hand, the low-frequency patterns of variability were shown to influence the type and frequency of RWB. For example, the frequency of AWB and CWB can be modulated by midlatitude weather regimes (Franzke et al., 2011; Swenson and Straus, 2017), the El Niño Southern Oscillation (ENSO) (Waugh and Polvani, 2000; Shapiro et al., 2001) or the Madden-Julian Oscillation (MJO) (Cassou, 2008). On the other hand, RWBs were shown to modify the low-frequency variability by triggering or extending the life-time of weather regimes (Michel and Rivière, 2011; Michel et al., 2012), and has an important role in the onset and decaying stages of blockings (Hoskins et al., 1983; Pelly and Hoskins, 2003; Woollings et al., 2008; Tyrlis and Hoskins, 2008; Woollings et al., 2011; Masato et al., 2012). More generally, a positive feedback was identified between RWBs and the latitudinal position of the jet, as a more poleward (equatorward) jet implies that AWB is more (less) probable (and vice versa for CWB), hence the jet is pushed or maintained further poleward (equatorward) by the eddy forcing (Rivière, 2009).

Moreover, it was suggested that the North Atlantic Oscillation (NAO), the leading mode of winter low-frequency variability in the North Atlantic region, can be viewed as variations in the frequency, type, and location of RWB events (Benedict et al., 2004; Rivière and Orlanski, 2007; Woollings et al., 2008; Strong and Magnusdottir, 2008; Kunz et al., 2009; Franzke et al., 2011). Generally, these studies find that AWBs (CWBs) are associated with the positive (negative) polarity of the NAO. Woollings et al. (2008) suggested that the negative NAO can be viewed as a period of more frequent high-latitude blocking events associated with CWB, resulting in a more zonal and southward jet regime, while the positive NAO can be viewed as period in which these events are infrequent, resulting in a more tilted and northward jet regime.

In addition, several previous studies have examined composites of RWB events. For example, Strong and Magnusdottir (2008) looked at composites of AWB and CWB events in the Northern Hemisphere (NH), and found that AWBs are associated with a negative (positive) Sea Level Pressure (SLP) anomaly poleward (equatorward) of the breaking, similar to the SLP signature of the positive NAO (and the opposite for CWB). Similar results were found by Kunz et al. (2009), who examined

https://doi.org/10.5194/egusphere-2023-534
Preprint. Discussion started: 23 March 2023
© Author(s) 2023. CC BY 4.0 License.

upper and lower tropospheric composites of RWB events in a simplified General Circulation Model (GCM), to study the potential of AWB and CWB events to drive NAO-like meridional circulation dipoles. Finally, Zhang and Wang (2018) examined composites of AWB in the North Atlantic during the warm season, to highlight the role of diabatic heating in contributing to the wave breaking.

Here we examine composites of RWB events in the North Atlantic during the winter season, but the focus is on relating the synoptic low-level cyclones and anticyclones to the time evolution of the upper-level breaking events. While the intrinsic relationship between weather systems and large-scale wave breaking events is well known, much of our knowledge is based on idealized studies (e.g., Simmons and Hoskins, 1978; Davies et al., 1991; Thorncroft et al., 1993). Michel et al. (2012) analyzed the link between surface cyclones and upper-tropospheric Rossby wave breaking during the Scandinavian Blocking (SB) regime. They found differing cyclones trajectories, associated with different types (cyclonic/anticyclonic) of wave breaking occurring during the onset and decay of the SB regime. Other studies have focused on how a precursor wave breaking can influence the cyclone's track and intensity. For example, the existence of simultaneous AWB and CWB events in the eastern North-Atlantic leads to a stronger and more zonally extended upper-level jet, which favors the formation of explosive storms reaching central Europe (Hanley and Caballero, 2012; Messori and Caballero, 2015). In addition, Gomara et al. (2014) examined the two-way relationship between RWB and explosive cyclones over the North Atlantic, and found that the latter are associated with enhanced frequency of RWBs several days prior to the cyclone's maximum intensification. They also found some signature for enhanced occurrence of CWB over southern Greenland and AWB over Europe after explosive cyclogenesis, but only for very intense cyclones.

Apart from the above mentioned studies, the intrinsic relation between the low-level cyclones, anticyclones, and RWB events has not been studied much, to the best of our knowledge. Here we highlight the fundamental relation between low-level weather systems and upper-level wave breaking events, focusing on the North Atlantic region. This is done by combining a Lagrangian feature-tracking technique (to identify and track low-level cyclones and anticyclones) with a wave-breaking detection algorithm (to identify the times and positions of cyclonic and anticyclonic RWB events). We show that anticyclones are intrinsically related to AWB, while cyclones are intrinsically related to CWB. However, both cyclones and anticyclones are involved with both types of wave breaking events. Moreover, the low-level storms have very different characteristics in each one of the RWB types, including strength, actual and relative positions, and tracks. In addition, composites of cyclones and anticyclones during the time evolution of the RWB events shows a relative anticyclonic (cyclonic) rotation during AWB (CWB) events. Finally, the eddy-mean flow interactions occurring in these breaking events are interpreted in terms of the observed synoptic evolution.

The paper is organized as follows. Section 2 reviews the data and methods used for the analysis, including the RWB detection algorithm, the Lagrangian storm-tracking technique, and the compositing procedure. In section 3, wave breaking-centered analysis is performed, and the fundamental relation between upper-level RWB events and low-level weather systems is presented, which shows the different characteristics of cyclones and anticyclones involved with AWB and CWB events. Section 4 presents the time-evolution of composites centered around anticyclones and cyclones during AWB and CWB, respectively, while section 5 examines anomalous life-cycles of cyclones during AWB and anticyclones during CWB events. Conclusion are discussed in section 6.

https://doi.org/10.5194/egusphere-2023-534
Preprint. Discussion started: 23 March 2023
© Author(s) 2023. CC BY 4.0 License.

2 Data and methods

In this study we use the six-hourly upper-level (250 hPa) horizontal velocities and Potential Vorticity (PV), PV on the 350K isentropic level, SLP, and lower-level (850 hPa) horizontal velocities and vorticity, from the European Centre for Medium-Range Weather Forecasts (ECMWF) interim reanalysis dataset (ERAI; Dee et al., 2011). The data covers the years 1980-2014 during the NH winter (December-January, DJF) period. Climatology is defined as the winter-average over these 35 years, while anomalies are defined as deviations from the DJF climatology. Note that the analysis is performed on the ERAI reanalysis data rather than on the newer ERA5 dataset for consistency between existing analyses of the tracking and wave-breaking detection results. However, we do not expect any major or fundamental differences in our conclusions if the ERA5 dataset was used instead.

2.1 Lagrangian storm-tracking algorithm

For the tracking of the low-level cyclones and anticyclones we use the objective feature-tracking algorithm TRACK of Hodges (1995, 1999), which is a widely used storm-tracking algorithm. We use the 850 hPa vorticity field, and the cyclone (anticyclone) centeres are then identified by a local maximum (minimum), with a cutoff of $1 \cdot 10^{-5}$ s^{-1} for the identification of the vorticity anomalies (a threshold customarily used for the identification of cyclones and anticyclones). The background flow is automatically removed by the algorithm prior to the tracking by subtracting all spatial wavenumbers smaller than or equal to 5, to isolate the synoptic-scale features. In addition, the vorticity field is reduced to a T42 grid, and then a spectral tapering is performed in order to suppress Gibbs phenomenon (Hodges, 1995). The centers of storms are tracked every six hours, and the tracking is performed on the sphere, by first initializing the maxima or minima into a set of tracks using a nearest neighbour method, and then refining these by performing a constrained minimization of a cost function for track smoothness (Hodges, 1999). The tracking is performed separately for cyclones and anticyclones, for each winter during the years 1980-2014 (where the year is defined according to January).

2.2 Rossby wave-breaking detection algorithm

The RWB detection algorithm used in this study is based on Strong and Magnusdottir (2008), and configured here to objectively identify the equatorward-breaking high-PV tongues associated with anticyclonically and cyclonically overturning PV contours. We use PV on the 350K isentropic level for the identification of RWB events, for each PV value between 1.5-7.5 PVU (similar results were also found by using PV on the 250 hPa level). This allows for detecting RWB in both lower and higher latitudes. The algorithm identifies large-scale overturning of circumpolar PV contours, on each one of the PV contours, by searching for contours crossing a particular meridian more than once. The algorithm uses the geometry of the overturning PV contour to quantify the zonal extent of the break and to distinguish between anticyclonic and cyclonic overturning (see Strong and Magnusdottir, 2008 for more details). In the original algorithm, the center of the breaking event is defined as the geographic centroid of the PV tongue (the equatorward PV tongue in our case). This is slightly modified here such that the latitudinal center of the event is chosen roughly between the poleward and equatorward PV tongues (for presentation purposes mainly).

https://doi.org/10.5194/egusphere-2023-534
Preprint. Discussion started: 23 March 2023
© Author(s) 2023. CC BY 4.0 License.

The latter is achieved by adding half of the meridional width of the tongue (at its centroid) to the centroid position. For each breaking event, only the spatially largest overturning is taken among the 1.5-7.5 PVU contours, and further events occurring less than L_x apart (L_x being the tongue's extent) are eliminated. In addition, if RWBs occur on adjacent days, only the day of maximum overturning is considered. The longitudinal width of an overturning AWB (CWB) is set to be larger than 7° (5°), the area of the breaking larger than $7 \cdot 10^{-4}$ as a fraction of earth's surface area, and the depth of the breaking (defined is the maximum PV value in the tongue minus the analyzed PV contour) is taken larger than 1 PVU. The spatial extent of the breaking events is chosen different for AWB and CWB, since the former are generally larger and greater in number, but similar qualitative results are obtained for other thresholds. Finally, only RWB events whose centroid lies within the Euro-Atlantic domain, defined here as the box (15N-75N, 80W-20E) are considered.

Examples of AWB and CWB events detected by the algorithm are shown in Fig. 1a and Fig. 1b, respectively. As can be seen in these examples, AWB (Fig. 1a) involves a high-PV streamer wrapping anticyclonically around a low-PV ridge. The AWB centroid is located in the equatorward (i.e. anticyclonic) side of the upper-level zonal flow, and the orientation of the PV contours is SW-NE. In contrast, CWB (Fig. 1b) involves the cyclonic wrapping of low-PV around a high-PV trough, and the orientation of the PV contours is SE-NW. In addition, the centeroid of the CWB is located in the poleward (i.e., cyclonic) side of the upper-level zonal flow. The position and tracks of the low-level cyclones and anticyclones are strongly related to these braking events, but it is difficult to identify any such relations from isolated examples. A deeper investigation of the relation between RWB events and low-level storms is given in Sections 3 and 4.

The normalized Probability Density Function (PDF) of the RWB centroids, shown in Fig. 1c,d, recovers well-known results for the distribution of the AWB and CWB positions. Namely, that AWB events (Fig. 1c) occur more in the downstream region of the Atlantic ocean basin (maximizing over western Europe), and mostly in the anticyclonic side of the time-mean Atlantic jet, while CWB events (Fig. 1d) occur more in the upstream region of the Atlantic ocean, mainly in the cyclonic side of the time-mean Atlantic jet. A secondary maximum in CWB is also found poleward of the African-Asia jet, but in the following analysis we only consider CWB occurring to the west of of 350° (i.e., in the upstream region of the Atlantic storm track), although our results do not change qualitatively if all CWB are considered instead.

Note that we have initially tested a RWB detection algorithm similar to the one used in Ndarana and Waugh (2010) and Garfinkel and Waugh (2014), and found qualitatively similar results (see Fig. S1 and Fig. S2 in the SI). However, unexpected extensive CWB activity was detected in the region where AWB is most frequent (Fig. S3), which is why an alternative algorithm was eventually used. Nonetheless, the equivalency of the results using the two different methods gives confidence in our results.

2.3 Composites of RWB events

The RWB identification algorithm and the storm-tracking results are used to construct composites of the flow during breaking events, centered either around the centroids of the breakings, or around the corresponding cyclones and anticyclones (see text in Section 4 for details). The breaking events are first separated into AWB events and CWB events, and composites are then constructed by placing a box sized 60 degrees in latitude by 70 degrees in longitude around the breaking centroid. This is performed separately for all AWB and CWB events, which are then averaged together for each type of breaking. Overall, there

https://doi.org/10.5194/egusphere-2023-534
Preprint. Discussion started: 23 March 2023
© Author(s) 2023. CC BY 4.0 License.

are 2,852 AWB events and 1,614 CWB events which satisfy the criterions in Section 2b, and are used for the breaking-centered composites

For the storm-ceneterd composites, similar criterions are used, but the composites are now centered around the closest anticyclone (for AWB events) or cyclone (for CWB events), within a 25 degree distance from the breaking centroid. Note that in order to fit the meridional extent of the composite box (30 degrees to the north and to the south of the composite center), in practice only RWB events or storms whose center is between 30N-60N are kept for the compositing. Overall, 2,085 anticyclones and 1,314 cyclones are identified as closest within a 25 degree distance from the breaking centroid of AWB and CWB events, respectively, and are used for storm-centered composites.

Additional composites representing anomalous life-cycles are also performed around anticyclones that reside to the east (E) of the breaking centroid for CWB, and around cyclones that reside either 5° to the north (N) or 5° to the south (S) of the breaking centroid for AWB. These choices are motivated by the results presented in Fig. 3, and will become clearer later. The $\pm 5^\circ$ criterion is used here to insure separation (due to the NW/SE orientation of the relative cyclone positions during AWB events), but results are not sensitive to this criterion. Overall, there are 1,281 (1,177) cyclones found to the N (S) of the breaking centroid of AWB, and 417 anticyclones found to the NE of the breaking centroid of CWB, which are used for the anomalous life-cycle composites presented in Section 5.

3 RWB events and their relation to low-level weather systems

3.1 Composites of breaking-centered RWB events

We first examine the wave breaking-centered composites of the upper and lower-level flows at the time of maximum breaking. Consistent with previous studies (e.g., Strong and Magnusdottir, 2008; Kunz et al., 2009), and similar to the example cases shown in Fig. 1, the composite of AWB events (Fig. 2a,b) show a high PV tongue (trough) wrapping anticyclonically around a low-PV (ridge) with a SW-NE orientation (Fig. 2a). The composite of the upper-level zonal flow (Fig. 2b) shows a split jet structure, with a tilted jet in the upstream region, poleward of the AWB center, and a strong decelerated region close to the breaking center. The upstream tilted structure is consistent with the notion that AWB are associated with a poleward shifted jet. However, there is also an additional downstream zonal and more equatorward jet, whose importance has been mentioned in the context of Mediterranean cyclones (e.g., Flaounas et al., 2015), and is associated with the African-Asian jet. The split jet structure during AWB will be discussed further when investigating the time-evolution composites in Section 4. The composite of CWB events (Fig. 2c) show a low-PV (ridge) wrapping cyclonically around a high-PV (trough), with a general SE-NW orientation. The composite of the upper-level zonal flow during CWB events shows a more zonal and southward jet, which is also slightly deccelerated close to the breaking center (Fig. 2d).

Also shown in Fig. 2 are the composite low-level (850 hPa) vorticity anomaly (black contours in Fig. 2a,c), and SLP anomaly (black contours in Fig. 2b,d). The anomalous SLP composites during AWB recover the results found by Strong and Magnusdottir (2008) and Kunz et al. (2009), with a negative SLP anomaly generally to the north of a positive SLP anomaly (similar to the positive NAO SLP dipole). Similar results are found for the 850 hPa vorticity composites (Fig. 2a), with a strong

https://doi.org/10.5194/egusphere-2023-534
Preprint. Discussion started: 23 March 2023
© Author(s) 2023. CC BY 4.0 License.

negative anticyclonic vorticity below and slightly to the east of the upper-level ridge, and a positive cyclonic vorticity to its north-northwest. The vorticity composites of AWB events also show an additional weaker cyclonic signature to the south of the anticyclonic vorticity, not seen in the SLP composites. We note that the current RWB detection algorithm identifies the breaking maximum in a relatively mature and developed stage, which is why the vorticity anomalies during AWB appear more N-S oriented rather than NW-SE. The initially used RWB detection algorithm (Ndarana and Waugh, 2010 and Garfinkel and Waugh, 2014), which detects breaking at an earlier stage, highlighted more strongly the NW-SE orientation (e.g., see Fig. S1 and Fig. S2). For CWB (Fig. 2b) we find, consistent with Strong and Magnusdottir (2008) and Kunz et al. (2009), a positive SLP anomaly to the N-NE of a negative SLP anomaly (generally similar to the negative NAO SLP dipole). The vorticity composites during CWB (Fig. 2d) show a strong cyclonic anomaly below and slightly to the east of the upper-level trough, and an anticyclonic anomaly to its NE.

To examine whether these pressure and vorticity anomalies are just signatures of the large-scale flow, or whether they are associated with the synoptic-scale cyclones and anticyclones themselves, we next utilize the storm-tracking algorithm to investigate the characteristics of low-level storms during RWB events.

3.2 Low-level weather systems during RWB events

The relation between upper-level RWB and low-level storms is first investigated by examining the relative positions, intensities, and propagation characteristics of the storms during RWB events. In the following analysis (presented in Fig. 3-Fig. 5) we use all the cyclones and anticyclones identified within a 25° distance from the breaking centroid (and not just the closest features, as done for the composite analysis). Overall, there are 5,106 (3,120) cyclones, and 4,136 (2787) anticyclones found during AWB (CWB).

Fig. 3 shows scatter plots of the positions of cyclones (left column) and anticyclones (right column) during RWB events, where color denotes the intensity of the system (in units of $10^{-5}\mathrm{s}^{-1}$), relative to the center of the AWB (Fig. 3a,b) and CWB (Fig. 3c,d). Clear signatures of preferred relative positions arise in these aggregated scatter plots. During AWB events (Fig. 3a,b), anticyclone locations are mostly below the upper-level ridge, close and slightly to the north of the AWB center (denoted by the cross symbol), while two distinct locations emerge for cyclones; strong cyclones are typically found to the N-NW of the breaking center, and a secondary region of weaker cyclones is found to the S-SE of the breaking center. Hence, AWBs are often associated with a cyclone-anticyclone-cyclone tripole, consistent with the vorticity composites shown in Fig. 2a. During CWB events (Fig. 3c,d), cyclones are typically found at low-levels close to the trough region, slightly to the SW of the CWB center. Consistent with the vorticity composites shown in Fig. 2c, anticyclones during CWB reside generally to the E-NE of the cyclones.

Additional information can be gained by plotting the actual positions, in physical space, of the storms during RWB events (Fig. **??**). The thick black contours show the normalized PDF of the storm counts (calculated using a kernel density estimator), highlighting the locations where storms are most observed. These PDFs are calculated for cyclones with magnitudes greater than $4 \cdot 10^{-5}\mathrm{s}^{-1}$ (Fig. **??**a,c), and for anticyclones with magnitudes greater than $3 \cdot 10^{-5}\mathrm{s}^{-1}$ (Fig. **??**b,d).

https://doi.org/10.5194/egusphere-2023-534
Preprint. Discussion started: 23 March 2023
© Author(s) 2023. CC BY 4.0 License.

Cyclones during AWB events (Fig. **??**a) are spread more equally over the Atlantic ocean basin, with notably more cyclones reaching the UK and Scandinavia, compared to cyclones during CWB (Fig. **??**c). A secondary peak in the cyclones' PDF is found over the Mediterranean. These Mediterranean cyclones, which generally reside to the S-SE of the AWB center, are much weaker compared to cyclones to the NW of the AWB center, and also compared to cyclones during CWB events (Fig. 5a). During CWB (Fig. **??**c), cyclones are concentrated more in the western side of the ocean basin. These cyclones, as expected, are located close to the region where CWB is maximum.

The cyclones also have very distinct propagation characteristics, depending on the type of breaking (cyclonic/anticyclonic), and their position relative to the breaking center. Fig. 5b,c shows the longitudinal and latitudinal displacements of cyclones during the four days centered around the breaking (i.e., the difference between the position two days after the breaking, r_{b+2}, minus the position two days prior the breaking, r_{b-2}; $\Delta r = r_{b+2} - r_{b-2}$). Cyclones during CWB (solid black line in Fig. 5b,c) mostly propagate eastward and poleward, as expected (e.g., Tamarin and Kaspi, 2016). However, separating cyclones during AWB into those occurring to the N and to the S of the AWB center reveals some interesting results. While cyclones to the N (dashed red lines in Fig. 5b,c) also tend to move eastward and poleward, cyclones to the S (dash-dotted blue lines in Fig. 5b,c) are much more stationary zonally and meridionally, and even propagate on average slightly equatorward. The hindering of the eastward and poleward propagation of these weaker cyclones is probably related to the anticyclonic (southwestward) wrapping of the trough around the ridge observed during AWB events (as will be shown in Fig. 6). This interesting feature should be investigated further, especially since it has been previously suggested that Mediterranean cyclones are dynamically linked to AWB in the Atlantic region (Flaounas et al., 2015; Raveh-Rubin and Flaounas, 2017).

Anticyclones during AWB and CWB events have similar intensities and propagation characteristics (Fig. 5d,f). However, anticyclones during AWB have slightly larger eastward displacement compared to anticyclones during CWB (an averaged longitudinal displacement of 31.2° compared to 27.8°, respectively). Consistently, anticyclones during AWB are found more in the downstream region of the storm track, while those associated with CWB are more in the upstream region and generally found at higher latitudes.

In the next section we examine the time evolution of these low-level cyclones and anticyclones during RWB events. Motivated by Fig. 3, we composite the flow around the anticyclones for AWB events and around cyclones for CWB events, as these occur closest to the breaking center in each case. This choice will be further supported by the similarity between the storm-centered composites and the breaking-centered composites, as shown next.

4 Time evolution of storm-centered composites during RWBs

The time evolution of RWB events is investigated by performing composites relative to the center of anticyclones for AWB, and relative to the center of cyclones for CWB. The advantage of compositing the flow around the storms is that we have information about their tracks, and can therefore investigate the time evolution of the flow leading to the event, even before the breaking had a signature that can be identified by the RWB detection algorithm.

https://doi.org/10.5194/egusphere-2023-534
Preprint. Discussion started: 23 March 2023
© Author(s) 2023. CC BY 4.0 License.

Fig. 6a-e and Fig. 8a-e show composites of the upper-level PV anomaly and the low-level SLP anomaly (in contours), centered around the anticyclones for AWB and around the cyclones during CWB, from $T = -3$ days prior to the breaking and up to $T = 2$ days after the breaking. During the time of maximum breaking ($T = 0$, Fig. 6c and Fig. 8c), the composites show a structure similar to that obtained by centering the flow on the wave breaking (shown in Fig. 2). The signal of the upper-level breaking (e.g., characterized by the overturning of the PV contours), is slightly weaker in the storm-relative composites, as expected. However, the results are otherwise similar, and capture the different cyclone/anticyclone orientations found for AWB and CWB events. We refer to these composites as the canonical cases, as they are more representative of the life-cycle of anticyclones and cyclones in the North Atlantic, obtained by compositing the flow around the storms, regardless of whether an upper-level RWB event has occurred (see Fig. S4 and Fig. S5, respectively). In the next two subsection we examine these life-cycles for AWB and CWB in detail, and in the next section the canonical cases are also compared with composites centered around cyclones during AWBs, and around anticyclones during CWBs, which represent anomalous cases.

4.1 Anticyclonic Wave Breaking

The time evolution of composites centered around the anticyclones during AWB (Fig. 6a-e) reveals some interesting features. Three days prior to the breaking ($T = -3$ days, Fig. 6a), there is a strong low-level anticyclone, residing to the east of an upper-level ridge. Importantly, both the ridge and the anticyclone reside in the anticyclonic side of the upper-level jet (Fig. 6f). There is also a weaker low-level cyclone, initially to the west of the anticyclone. Note that the strong low-level anticyclone is obviously due to the centering of the composites around the anticyclones. Compositing the flow around the cyclones instead will be discussed in Section 5, but we note here that this still gives a strong anticyclonic circulation at upper-levels (e.g., Fig. 9d-i).

Both the anticyclone and the cyclone to its west slightly intensify during the build-up of the wave breaking (Fig. 6a,b). In addition, the cyclone rotates in an anticyclonic manner relative to the anticyclone (Fig. 6a-e), eventually merging with a negative SLP anomaly initially to the northeast of the anticyclone. Parallel to this, the upper-level trough to the east (downstream) of the ridge is wrapped around the ridge and the classical picture of wave breaking and inversion of meridional PV gradient is found (i.e., a negative PV anomaly to the north of a positive PV anomaly). During the decay stage of the wave breaking (Fig. 6d,e), the anticyclone slightly weakens and the flow becomes more barotropic, and two days after the breaking maximum ($T = 2$ days, Fig. 6f), the low pressure anomaly is entirely to the north of the anticyclone. The low-level positive NAO-like pressure dipole (the low-above-high pressure anomalies) is in agreement with Strong and Magnusdottir (2008) and Kunz et al. (2009), but here the time-evolution of the low-level cyclones and anticyclones leading to this structure is examined.

During the evolution of the breaking, the total upper-level zonal flow (Fig. 6f-j) weakens significantly to the south of the ridge, while the downstream zonal and more southward jet intensifies. Hence, the initially more wavy-like upper-level jet (Fig. 6f) is split into an upstream tilted jet, and a downstream zonal jet (Fig. 6h). The split jet structure has been noted in several previous studies examining Mediterranean cyclones and their relation to AWB (e.g., Flaounas et al., 2015; Raveh-Rubin and Flaounas, 2017). However, it is not usually discussed in relation to the classical theories concerning the poleward shift of the jet in AWB. Separating the total flow into a time-mean (in this case the climatological DJF mean over all the years)

https://doi.org/10.5194/egusphere-2023-534
Preprint. Discussion started: 23 March 2023
© Author(s) 2023. CC BY 4.0 License.

and an anomalous flow, i.e., $u = \overline{u} + u'$ (where an overline represents time-mean and prime represents deviation from that time-mean) shows that it is mainly the time-mean flow that contributes to the downstream jet (note that the composites of the time-mean flow vary with time here since the compositing is centered around the storms which are moving, hence at different locations with respect to the Eulerian time-mean flow, see Fig. S6 in the SI). The downstream jet is therefore probably linked to the time-mean subtropical Asian-African jet, as the storm approach the eastern side of the ocean basin.

The negative upper-level meridional velocity between the ridge and the trough to its east (Fig. 6k-o) increases significantly during the breaking, and is mainly due to the intensifying anomalous ridge-trough system (see also Fig. S6k-o in the SI for the anomalous meridional velocities). Similarly, the negative anomalous zonal velocity between the ridge and the trough which is breaking anticyclonically to its south is also intensifying (see also Fig. S6f-j in the SI for the anomalous zonal velocities) This anomalous southwestward upper-level velocity is contributing to the breaking of the wave by advecting the anomalous upper-level trough southward and westward around the ridge. This nonlinear advection reinforces the upper-level anticyclonic rotation due to the background anticyclonic shear. In addition, the anomalous upper-level anticyclonic circulation associated with the ridge induces a relative anticyclonic rotation at low-levels (through interaction between the upper and lower levels PV anomalies, not shown), as it acts to advect the low-level anticyclone equatorward and the cyclone to its west poleward (see SLP anomalies and arrows representing the anomalous circulation in Fig. 6a-e), in general agreement with Tamarin and Kaspi, 2016.

Fig. 7a-c shows cross sections of the upper-level zonal velocity at the longitude crossing the center of the composite box (i.e., the center of the anticyclone) . The peak of the total upper-level zonal flow initially increases slightly and then decreases, while the relative latitude at which this peak is achieved remains roughly the same (Fig. 7a, see changes in the lines going from black, denoting $T = -3$ days, to blue, denoting $T = 2$ days). Southwards of peak in total U, the zonal flow decreases significantly during the breaking, and a secondary peak develops further southward. The strong deceleration of U southward of the anticyclone center is related to the intensification of the negative anomalous zonal velocity (Fig. 7b), due to the intensifying ridge and the anticyclonically wrapping trough to its south. The climatological (time-averaged) zonal velocity (Fig. 7c) also contributes to the apparent weakening of U, due to the motion of the storms into a region where the time-mean Atlantic jet is weaker, while it contributes to the strengthening of the total U more southward (a signature of the downstream subtropical jet). These changes in the time-mean jet are related to the eastward propagation of the anticyclones, as they propagate away from the Atlantic jet and approach the downstream exit region of the storm track. Note that the anticyclones are also propagating meridionally. Taking into account the averaged latitudinal displacement of the anticyclones at each time-step (which is poleward in this case, see Fig. 5d), shows that the peak in the total upper-level U is shifted poleward (see Fig. S8a in the SI).

The results above are consistent with the usual notion that AWB events are associated with a poleward shift of the zonal mean jet, due to the poleward momentum fluxes that result from the SW-NE tilt of the PV contours. Here we suggest an alternative mechanistic interpretation, in which the poleward shift is merely a result of the intensification and anticyclonic rotation of the ridge-trough system. The anomalous velocities associated with an intensifying ridge would contribute, in a zonally averaged sense, to a poleward shift of the jet (a strengthening of the total zonal flow poleward the ridge, and a weakening equatorward of it). However, for a linear wave, this effect will cancel out (in the zonal mean) with the adjacent trough, which will have

https://doi.org/10.5194/egusphere-2023-534
Preprint. Discussion started: 23 March 2023
© Author(s) 2023. CC BY 4.0 License.

the opposite net effect. The nonlinearity associated with the breaking results in a northeastward motion of the ridge and a southwestward motion of the downstream trough (i.e., a relative anticyclonic rotation). This breaks both the zonal and the meridional symmetries. First, it favors a negative meridional velocity between the ridge and the downstream trough. Second, it contributes to a negative anomalous zonal velocity between the ridge and the trough which is wrapping to its south. These anomalous velocities are not averaged out in the zonal mean in this case. Thus, overall, an intensifying and anticycloniclly breaking ridge-trough system results in an intensification (weakening) of the total zonal flow in the area northward (southward) of the breaking (see also the schematic shown in Fig. 10, for an illustration of the upper and lower level evolution during RWB, discussed in the conclusions).

4.2 Cyclonic Wave Breaking

We next examine the time evolution of composites centered around cyclones during CWB (Fig. 8a-e). Three days prior to the breaking ($T = -3$ days, Fig. 8a), there is a strong low-level cyclone, residing to the east of an upper-level trough, and poleward of an upper-level jet (i.e. in the cyclonic side, Fig. 8f). There are also weak signatures of an anticyclone to the west and to the north-northeast of the cyclone. During the build-up of the breaking (Fig. 8a-c), both the low-level cyclone and the upper-level trough intensify, while a downstream ridge and a low-level anticyclonic anomaly are intensifying to the east and north-east of the cyclone. A relative cyclonic rotation is observed both at upper and lower-levels, as the downstream ridge starts rotating in a cyclonic manner relative to the trough (Fig. 8b-d).

During the decay stage of the wave breaking (Fig. 8d,e) the ridge is weakened and dissipated out (see also black contours in Fig. 8n,o showing the PV anomaly). At low-levels, the cyclone becomes more barotropically aligned with the upper-level trough, and two days after the breaking maximum ($T = 2$ days, Fig. 8e) the high pressure anomaly is mostly to the north of the cyclone. These results are generally similar to Strong and Magnusdottir (2008), who examined composites of CWB and found a low-level negative NAO-like pressure dipole (a high-above-low pressure dipole), and to Kunz et al. (2009), who examined CWB in simplified GCM experiments and found a similar dipole at upper-levels (a low-above-high meridional PV anomaly dipole).

The total zonal flow (Fig. 8f-j) weakens in magnitude, most strongly to the north of the cyclone center, and its peak shifts southward relative to the cyclone center. The weakening and southward shift of the jet in the composites, which are observed also in the composites of the time-mean flow (Fig. S7a-e, see also Fig. 7d-f), are probably a result of the eastward and poleward motion of the cyclones, as they move further away from the time-mean flow and approach the weaker jet exit region. The anomalous upper-level zonal velocity (Fig. S7f-j and arrows in Fig. 8a-e), which is dominated by the upper-level trough, is positive to the south of the trough, but a strong negative anomalous zonal velocity is generated between the trough and the ridge which is breaking cyclonically to its north. Similarly, the positive upper-level meridional velocity between the trough and the ridge to its east, which is mostly due to the anomalous flow (Fig. S7k-o), increases during the evolution of the breaking, as the trough-ridge system grows (Fig. 8k-o). As in AWB, the anomalous upper-level velocity is contributing to the breaking, in this case by nonlinear northwestward advection of the ridge around the trough (i.e., in a cyclonic manner), which reinforces the rotation induced by the cyclonic shear.

https://doi.org/10.5194/egusphere-2023-534
Preprint. Discussion started: 23 March 2023
© Author(s) 2023. CC BY 4.0 License.

The cross sections of the upper-level zonal velocity at the longitude crossing the center of the cyclone (Fig. 7d-f) show that the peak of the total zonal flow (Fig. 7d) weakens and shifts southward throughout the life-cycle of the breaking. This is mainly due to the time-mean zonal flow (Fig. 7f), and is related to the eastward and poleward propagation of the cyclones away for the jet core. In addition, the flow weakens strongly poleward of the breaking. The latter is due to the intensification of the negative anomalous zonal velocity (Fig. 7e), related to the intensifying and cyclonically rotating ridge-trough system. Fixing the cross-sections by taking into account the averaged latitudinal poleward displacement of the cyclones at each time-step shows that in this case, the peak in the total upper-level U remains roughly at the same latitude (see Fig. S8b in the SI). This seems to suggest an interesting asymmetry between AWB and CWB events, namely that during AWB events, the already poleward shifted jet can shift even further poleward, while during CWB, the equatorward shifted jet is remains at a similar latitude.

Nonetheless, there is a clear weakening of the total upper-level jet poleward of the breaking during CWB, consistent with the notion that CWBs are associated with an equatorward shifted zonal mean jet, due to the equatorward momentum fluxes that result from the SE-NW tilt. Similar to AWB, we suggest that this is due to nonlinearity associated with the breaking (i.e., the cyclonic wrapping of the ridge around the trough) which breaks the zonal and meridional symmetries, as it favors a positive meridional velocity between the trough and the ridge to it east, and a negative anomalous zonal velocity between the trough and the breaking ridge to its north, which are not averaged out in the zonal mean (see also Fig. 10 for a schematic illustration of the upper and lower level evolution during RWB).

5 Anomalous life-cycles of cyclones and anticyclones

In section (4a) and (4b), the composites of anticyclones during AWB and cyclones during CWB events were presented. These largely resemble the life-cycles of anticyclones and cyclones (see Fig. S4 and Fig. S5 in the SI), regardless of the existence of an upper-level breaking event. For example, anticyclones (cyclones) reside, on average, on the anticyclonic (cyclonic) side of the shear, and an upper-level breaking in the corresponding sense is often found at upper-levels (Fig. S4 and Fig. S5). Hence, to examine whether our wave breaking composites are not merely influenced by the choice of anticyclones (cyclones) for AWB (CWB) events, we next investigate the same composites, but now centered around anticyclones during CWB (to the NE of the CWB center), and around cyclones during AWB events, where the later is separated into cyclones residing to the N or S of the AWB center (and similar results are found if the separation is into cyclones residing to the NW or SE of the AWB center).

5.1 Anticyclones during CWB

Compositing the flow around anticyclones during CWB (Fig. 9a-c) shows that they are located now to the north of the zonal jet (i.e., in the cyclonic shear), even two days prior to the breaking (Fig. 9a). These composites are dominated by an upper-level ridge, and a low-level anticyclone with a weaker cyclone to its SW (similar to the orientation found in the CWB composites). Although the anomalous upper-level velocity is dominated by the anticyclonic circulation, the cyclone and anticyclone still rotate in a cyclonic manner relative to each other (now it is the cyclone that rotates cyclonically around the anticyclone, due to the centering of the composites around the anticyclones). Similarly, the deepening trough seen to the west of the anomalous

https://doi.org/10.5194/egusphere-2023-534
Preprint. Discussion started: 23 March 2023
© Author(s) 2023. CC BY 4.0 License.

ridge (see the 2.5 PVU contour) is clearly not a result of advection associated with the anomalous upper-level anticyclonic circulation, which is in the opposite sense. One day after the breaking maximum (not shown), signatures of AWB start to develop in the downstream region of the ridge.

These anticyclone-centered composites reveal an anonalous life-cycle, quite different from the more canonical life-cycle of anticyclones (Fig. S4 and Fig. 6 for anticyclones during AWB). In both types of life-cycles, the anticyclone is initially to the east of the cyclone. However, crucially, the anticyclone is in the anticyclonic side of the jet in AWB (and slightly to the SE of the cyclone), and in the cyclonic side of the jet in CWB (and slightly to the NE of the cyclone). The background cyclonic shear reinforces the developing trough, and by $T = 0$ a strong cyclonic circulation is evident at upper-levels (a SW-NE tilted trough-ridge dipole), with strong negative momentum fluxes between the trough and the ridge (consistent with the equatorward shifted jet in the upstream region.

5.2 Cyclones during AWB

For AWB, we separate the composites into those centered around cyclones to the north (N) (Fig. 9d-f) and to the south (S) (Fig. 9g-i). In both cases, the upper-level flow is still dominated by an upper-level ridge (similar to what was found when compositing around the anticyclones during AWB), even though the compositing is performed on the cyclones. For cyclones to the N (Fig. 9d-f), prior to the breaking, a strong low-level cyclone is found with an anticyclone to its SE, the latter residing on the equatorward (anticyclonic) side of the jet. Even though the low-level cyclone is stronger than the anticyclone, the cyclone-anticyclone dipole rotate in an anticyclonic manner relative to each other (this time it is the anticyclone that rotates anticyclonically around the cyclone, due to the centering of the composites around the cyclones). This anticyclonic rotation is entirely due to the dominance of the ridge at upper-levels, and is in stark contrast to the low-level cyclonic circulation and the usual cyclonic wrap-up seen at upper-levels during the life-cycle of cyclones (Fig. S5). The strong upper-level ridge ultimately leads to an anticyclonic breaking in the downstream region, by contributing to the growth and anticyclonic breaking of the trough to the east of the ridge. Note that the breaking signal is very weak due to the centering of the flow over the cyclones, which are not necessarily close to the breaking center.

Finally, centering the flow around cyclones to the S of the AWB center (Fig. 9g-i) gives, prior to the breaking, a strong upper-level ridge and a weaker upper-level trough to its SE. The low-level anticyclone-cyclone dipole (as well as the upper-level ridge-trough dipole) rotates in an anticyclonic manner relative to each other, with the anticyclone becoming ultimately to the north of the cyclone. This contributes to the strong deceleration of the zonal flow southward of the ridge, as discussed in Section 4a. Hence, although these cyclones reside in the cyclonic side of an upper-level (more zonal and southward) jet, they are mostly influenced by the anticyclonic shear associated with the strong upstream ridge. These cyclones, which are significantly weaker than the cyclones to the N of the AWB, are probably generated as a secondary-development from the breaking upper-level trough (PV streamer). As seen in Fig. **??**a, these cyclones are mostly in the Mediterranean region. Indeed, it has been suggested that PV streamers associated with AWB in the Atlantic could be a key process for the development of Mediterranean cyclones (Flaounas et al., 2015; Raveh-Rubin and Flaounas, 2017). The similarity between the storm-relative composites for cyclones to the S of AWB and Fig. 10 of Flaounas et al. (2015), showing storm-centered composites for

https://doi.org/10.5194/egusphere-2023-534
Preprint. Discussion started: 23 March 2023
© Author(s) 2023. CC BY 4.0 License.

the 200 most intense Mediterranean cyclones, is remarkable. This encourages further research on the growth, dynamics, and propagation characteristics of Mediterranean cyclones, which would potentially be very different from the canonical cases of Atlantic cyclones.

6 Conclusions

This study examines the fundamental relationship between upper-level Rossby wave breaking events and low-level cyclones and anticyclones. This is achieved by combining a Rossby wave breaking detection algorithm with a storm-tracking technique. The different life-cycles and characteristics of cyclones and anticyclones during AWB and CWB events are examined, by investigating the positions, intensities and propagation characteristics of the storms, as well as by constructing storm-centered composites to examine the time evolution during each type of breaking.

The main results and conclusions can be summarized as follows:

1) During AWB, a low-level anticyclone is found close and slightly to the N of the breaking center. However, two preferred locations of cyclones relative to the center of the breaking emerge, to the S-SE and to the N-NW of the anticyclone. Overall, the orientation of the cyclone-anticyclone-cyclone tripole is SE-NW during the breaking development stage, and becomes more S-N oriented by the end of the life-cycle. Geographically, cyclones to the N-NW of AWB are spread more over the upstream and mid-Atlantic ocean basin, while cyclones to the S-SE (which are generally much weaker) are found more over the eastern coast and the Mediterranean region. The propagation characteristics of these two groups of cyclones differ significantly; while the cyclones to the N-NW propagate on average eastward and poleward, as expected, cyclones to the S-SE of AWB propagate much less zonally and meridionally (almost stationary).

2) During CWB, a strong low-level cyclone is usually found close to the CWB center, while anticyclones are found to the NE of the cyclones, such that the cyclone-anticyclones dipole has a SW-NE orientation. Geographically, cyclones during CWB are found mostly close to the western coast of the North Atlantic ocean basin, and generally reach higher latitudes. Anticyclones are located more downstream, close to the Eastern ocean basin, and generally to the NE of the cyclones.

3) The time evolution of composites centered around anticyclones during AWB events shows, prior to the breaking, a low-level anticyclone to the east of a strong upper-level ridge (i.e., with a baroclinic structure), which resides in the anticyclonic side of the jet (see Fig. 10 for a schematic illustration of the upper and lower flow evolution). A low-level cyclone is found initially to the west of the anticyclone, and during the evolution of the breaking the cyclone-anticyclone pair rotate in an anticyclonic manner relative to each other, such that we find a negative SLP poleward of a positive SLP anomaly by the end of the life-cycle. At upper-levels, the trough to the east of the initial ridge grows and then wraps anticyclonically around the ridge. Consistently, the upper-level jet is split into an upstream tilted jet, and a downstream zonal and more southward jet. In this case, the anomalous anticyclonic circulation associated with the ridge is acting to reinforce the anticyclonic shear, contributing to the anticyclonic rotation of the system.

4) The time evolution of composites centered around cyclones during CWB events shows, prior to the breaking, a low-level cyclone to the east of a strong upper-level trough, which resides in the cyclonic side of the jet (see Fig. 10). A low-

https://doi.org/10.5194/egusphere-2023-534
Preprint. Discussion started: 23 March 2023
© Author(s) 2023. CC BY 4.0 License.

level anticyclone is found initially to the west of the cyclone, which weakens and disappears while rotating cyclonically (southeastward) around the cyclone. An additional low-level anticyclone and an upper-level ridge develop downstream, to the east of the cyclone, and during the evolution of the breaking the whole system rotates in a cyclonic manner relative to each other, such that a positive SLP anomaly is found poleward of a negative SLP anomaly by the end of the life-cycle. As the ridge wraps cyclonically around the trough, a strong negative anomalous velocity is generated, such that the total zonal flow is decelerated poleward of the breaking center. The anomalous cyclonic circulation associated with the upper-level trough is acting to reinforce the cyclonic shear, contributing to the cyclonic rotation of the system.

5) An alternative interpretation is suggested here for the poleward (equatorward) shifted jet associated with AWB (CWB) events, in which the shift is merely a result of the anticyclonic (cyclonic) rotation of the ridge-trough (trough-ridge) system. To see this, consider a linear wave composed of ridges and troughs superimposed on a background jet. While each anomalous ridge could contribute, in a zonally averaged sense, to a poleward shift of the jet by strengthening the total zonal flow poleward the ridge, and weakening equatorward of it (and opposite for an anomalous trough), a linear wave composed of ridges and troughs, would not contribute to any net shifts of the zonal mean jet, since these effects would cancel out. However, the nonlinearity results in an anticyclonic wrapping of the trough around the ridge for AWB, and a cyclonic wrapping of the ridge around the trough for CWB, which breaks the zonal and meridional symmetries. For AWB, it favors a negative anomalous meridional velocity between the ridge and the trough to its east, and a negative anomalous zonal velocity due to the anticyclonic rotation of the trough around the ridge (i.e., to its southeast). For CWB, it favors a positive anomalous meridional velocity between the trough and the ridge to its east, and a negative anomalous zonal velocity due to the cyclonic rotation of the ridge around the trough (i.e., to its northeast). Crucially, these anomalous southwestward and northwestward velocities (for AWB and CWB, respectively) do not average out in the zonal mean. Note that these anomalous velocities ($v' < 0$ and $u' < 0$ for AWB and $v' > 0$ and $u' < 0$ for CWB), are exactly those that constitute the positive (negative) momentum fluxes, which theoretically are associated with a poleward (equatorward) shift of the mean zonal jet in AWB (CWB).

Nonetheless, taking into account the latitudinal motion of the storms shows that while AWB events indeed end-up with a more poleward shifted upper-level jet, the jet during CWB seem to remain at the same (equatorward shifted to begin with) latitude.

6) Anomalous life-cycles of cyclones and anticyclones are found, by centering the composites around the anticyclones during CWBs, and around cyclones during AWBs (where the latter is further separated into cyclones residing to the N or S of the AWB center). In all cases, the shear of the total upper-level zonal flow is determining the overall relative rotation, and therefore the type of breaking. For example, anticyclones during CWB reside in the 'wrong' (cyclonic) side of the jet, and therefore experience an atypical life-cycle. Cyclones to the S of the AWB center (e.g., over the Mediterranean region) are strongly influenced by an upper-level anticyclonic circulation, and therefore experience an atypical life-cycle of cyclones, which are usually dominated by an upper-level trough. This motivates further research on the propagation characteristics and growth mechanisms of Mediterranean cyclones compared to Atlantic cyclones.

The methods used in the current study can be easily applied to other regions, e.g., the Pacific storm track or the Southern Hemisphere storm track. It would be interesting to investigate if similar results are obtained, e.g., in a zonally symmetric

https://doi.org/10.5194/egusphere-2023-534
Preprint. Discussion started: 23 March 2023
© Author(s) 2023. CC BY 4.0 License.

storm track, or whether some of these findings are shaped by the stationary waves in the North Atlantic. Another interesting future direction is to incorporate circulation regimes in the North Atlantic, which are recurrent and persistent regimes of the atmospheric circulation, to examine more deeply the interaction among scales between the high frequency, synoptic-scale weather system, and the low-frequency circulation, and how it is mediated by RWB events. These are left for future studies.

Data availability. The ERA-Interim data used in this study has been obtained from the ECMWF data server: http://apps.ecmwf.int/datasets/

Author contributions. T.T.B. and N.H. designed the study and wrote the paper; T.T.B. performed the data analyses

Competing interests. The authors declare no competing interests.

Acknowledgements. This research has been supported by the Israeli Science Foundation (ISF) Research Grant no. 1685/17 and 2713/17 of Prof. Nili Harnik.

https://doi.org/10.5194/egusphere-2023-534
Preprint. Discussion started: 23 March 2023
© Author(s) 2023. CC BY 4.0 License.

References

Benedict, J. J., S. Lee, and S. B. Feldstein, 2004: Synoptic view of the north atlantic oscillation. *Journal of the Atmospheric Sciences*, **61**, 121–144.

Cassou, C., 2008: Intraseasonal interaction between the madden-julian oscillation and the north atlantic oscillation. *Nature*, **455**, 523–527.

Charney, J., 1947: The dynamics of long waves in a baroclinic westerly current. *J. Meteor*, **4 (5)**, 135–161.

Davies, H. C., C. Schar, and H. Wernli, 1991: The palette of fronts and cyclones within a baroclinic wave development. *J. Atmos. Sci.*, **48**, 1666–1689.

de Vries, A. J., 2021: A global climatological perspective on the importance of rossby wave breaking and intense moisture transport for extreme precipitation events. *Weather and Climate Dynamics*, **2**, 129–161.

Dee, D. P., and Coauthors, 2011: The ERA-Interim reanalysis: configuration and performance of the data assimilation system. *Q. J. R. Meteorol. Soc.*, **137**, 553–597.

Eady, E., 1949: Long waves and cyclone waves. *Tellus*, **1 (3)**, 33–52.

Flaounas, E., S. Raveh-Rubin, H. Wernli, P. Drobinski, and S. Bastin, 2015: The dynamical structure of intense mediterranean cyclones. *Climate Dynamics*, **44**, 2411–2427.

Franzke, C., T. Woollings, and O. Martius, 2011: Persistent circulation regimes and preferred regime transitions in the north atlantic. *J. Atmos. Sci.*, **68**, 2809–2825.

Gabriel, A., and D. Peters, 2008: A diagnostic study of different types of rossby wave breaking events in the northern extratropics. *Journal of the Meteorological Society of Japan*, **86**, 613–631.

Garfinkel, C. I., and D. W. Waugh, 2014: Tropospheric rossby wave breaking and variability of the latitude of the eddy-driven jet. *Journal of Climate*, **27**, 7069–7085.

Gomara, I., J. G. Pinto, T. Woollings, G. Masato, P. Zurita-Gotor, and B. Rodríguez-Fonseca, 2014: Rossby wave-breaking analysis of explosive cyclones in the euro-atlantic sector. *Quarterly Journal of the Royal Meteorological Society*, **140**, 738–753.

Hanley, J., and R. Caballero, 2012: The role of large-scale atmospheric flow and rossby wave breaking in the evolution of extreme windstorms over europe. *Geophys. Res. Lett.*, **39**, L21 708.

Hartmann, D. L., 2000: The key role of lower-level meridional shear in baroclinic wave life cycles.

Hartmann, D. L., and P. Zuercher, 1998: Response of baroclinic life cycles to barotropic shear.

Hodges, K. I., 1995: Feature tracking on the unit sphere. *Mon. Weather Rev.*, **123 (12)**, 3458–3465.

Hodges, K. I., 1999: Adaptive constraints for feature tracking. *Mon. Weather Rev.*, **127 (6)**, 1362–1373.

Hoskins, B., I. James, and G. White, 1983: The shape, propagation and mean–flow interaction of large–scale weather systems. *J. Atmos. Sci.*, **40**, 1595–1612.

Kunz, T., K. Fraedrich, and F. Lunkeit, 2009: Synoptic scale wave breaking and its potential to drive nao-like circulation dipoles: A simplified gcm approach. *Quarterly Journal of the Royal Meteorological Society*, **135**, 1–19.

Martius, O., and G. Rivière, 2016: Rossby wave breaking: climatology, interaction with low-frequency climate variability, and links to extreme weather events. *Dynamics and Predictability of Large-Scale, High-Impact Weather and Climate Events*, 69–78.

Masato, G., B. J. Hoskins, and T. J. Woollings, 2012: Wave-breaking characteristics of midlatitude blocking. *Q. J. R. Meteorol. Soc.*, **138**, 1285–1296.

McIntyre, M. E., and T. N. Palmer, 1983: Breaking planetary waves in the stratosphere. *Nature*, **305**, 593–600.

https://doi.org/10.5194/egusphere-2023-534
Preprint. Discussion started: 23 March 2023
© Author(s) 2023. CC BY 4.0 License.

Messori, G., and R. Caballero, 2015: On double rossby wave breaking in the north atlantic. *Journal of Geophysical Research*, **120**, 11,129–11,150.

Michel, C., and G. Rivière, 2011: The link between rossby wave breakings and weather regime transitions. *Journal of the Atmospheric Sciences*, **68**, 1730–1748.

Michel, C., G. Rivière, L. Terray, and B. Joly, 2012: The dynamical link between surface cyclones, upper-tropospheric rossby wave breaking and the life cycle of the scandinavian blocking. *Geophysical Research Letters*, **39**.

Moore, B. J., D. Keyser, and L. F. Bosart, 2019: Linkages between extreme precipitation events in the central and eastern united states and rossby wave breaking. *Monthly Weather Review*, **147**, 3327–3349.

Ndarana, T., and D. W. Waugh, 2010: The link between cut-off lows and rossby wave breaking in the southern hemisphere. *Quarterly Journal of the Royal Meteorological Society*, **136**, 869–885.

Orlanski, I., 2003: Bifurcation in eddy life cycles: Implications for storm track variability. *J. Atmos. Sci.*, 993–1023.

Pelly, J. L., and B. J. Hoskins, 2003: A new perspective on blocking. *J. Atmos. Sci.*, **60**, 743–755.

Peters, D., and D. W. Waugh, 1996: Influence of barotropic shear on the poleward advection of upper-tropospheric air. *Journal of the Atmospheric Sciences*, **53**, 3013–3031, https://doi.org/10.1175/1520-0469(1996)053<3013:IOBSOT>2.0.CO;2.

Raveh-Rubin, S., and E. Flaounas, 2017: A dynamical link between deep atlantic extratropical cyclones and intense mediterranean cyclones. *Atmospheric Science Letters*, **18**, 215–221.

Rivière, G., 2009: Effect of latitudinal variations in low-level baroclinicity on eddy life cycles and upper-tropospheric wave-breaking processes. *J. Atmos. Sci.*, **66**, 1569–1592.

Rivière, G., and I. Orlanski, 2007: Characteristics of the atlantic storm-track eddy activity and its relation with north atlantic oscillation. *Journal of the Atmospheric Sciences*, **64**, 241–266.

Shapiro, M., and Coauthors, 1999: A planetary-scale to mesoscale perspective of the life cycles of extratropical cyclones: The bridge between theory and observations. American Meteorological Society, 139-185 pp., https://doi.org/10.1007/978-1-935704-09-6_14.

Shapiro, M. A., H. Wernli, N. A. Bond, and R. Langland, 2001: The influence of the 1997-99 el nino southern oscillation on extratropical baroclinic life cycles over the eastern north pacific. *Q. J. R. Meteorol. Soc.*, **127**, 331–342.

Simmons, A., and B. Hoskins, 1978: The life cycles of some nonlinear baroclinic waves. *J. Atmos. Sci.*, **35 (3)**, 414–432.

Strong, C., and G. Magnusdottir, 2008: Tropospheric rossby wave breaking and the nao/nam. *Journal of the Atmospheric Sciences*, **65**, 2861–2876.

Swenson, E. T., and D. M. Straus, 2017: Rossby wave breaking and transient eddy forcing during euro-atlantic circulation regimes. *J. Atmos. Sci.*, **74**, 1735–1755.

Tamarin, T., and Y. Kaspi, 2016: The poleward motion of extratropical cyclones from a potential vorticity tendency analysis. *J. Atmos. Sci.*, **73**, 1687–1707.

Thorncroft, C. D., B. J. Hoskins, and M. E. McIntyre, 1993: Two paradigms of baroclinic wave life-cycle behaviour. *Quarterly Journal of the Royal Meteorological Society*, **119**, 17–55.

Tyrlis, E., and B. J. Hoskins, 2008: The morphology of northern hemisphere blocking. *Journal of the Atmospheric Sciences*, **65**, 1653–1665.

Waugh, D. W., and L. M. Polvani, 2000: Climatology of intrusions into the tropical upper troposphere. *Geophys. Res. Lett.*, **27**, 3857–3860.

Wittman, M. A. H., A. J. Charlton, and L. M. Polvani, 2007: The effect of lower stratospheric shear on baroclinic instability. *J. Atmos. Sci.*, **64**, 479–496.

https://doi.org/10.5194/egusphere-2023-534
Preprint. Discussion started: 23 March 2023
© Author(s) 2023. CC BY 4.0 License.

Woollings, T., B. Hoskins, M. Blackburn, and P. Berrisford, 2008: A new rossby wave-breaking interpretation of the north atlantic oscillation. *J. Atmos. Sci.*, **65**, 609–626.

Woollings, T., J. G. Pinto, and J. A. Santos, 2011: Dynamical evolution of north atlantic ridges and poleward jet stream displacements. *J. Atmos. Sci.*, **68**, 954–963.

Zhang, G., and Z. Wang, 2018: North atlantic extratropical rossby wave breaking during the warm season: Wave life cycle and role of diabatic heating. *Monthly Weather Review*, **146**, 695–712.

Zhang, G., Z. Wang, M. S. Peng, and G. Magnusdottir, 2017: Characteristics and impacts of extratropical rossby wave breaking during the atlantic hurricane season. *Journal of Climate*, **30**, 2363–2379.

https://doi.org/10.5194/egusphere-2023-534
Preprint. Discussion started: 23 March 2023
© Author(s) 2023. CC BY 4.0 License.

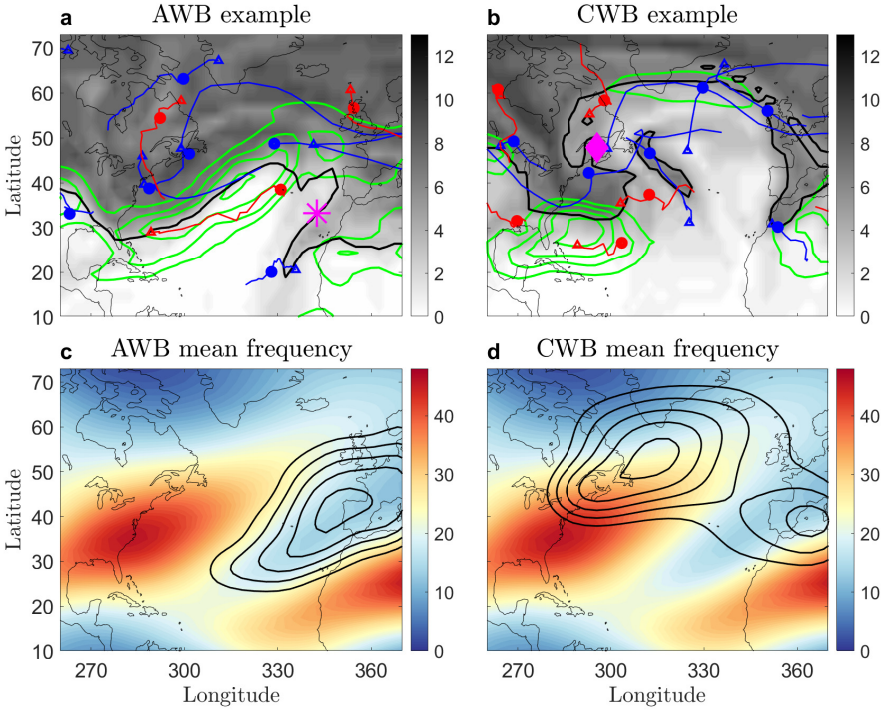

Figure 1. Examples of an (a) Anticyclonic Rossby Wave Breaking (AWB), and (b) Cyclonic Rossby Wave Breaking (CWB) event. Shown are the upper-level (250 hPa) Potential Vorticity (PV) in PV Units (PVU, 1 PVU=$10^{-6}\mathrm{Kkg}^{-1}\mathrm{m}^2\mathrm{s}^{-1}$) (grey shading), the 250 hPa zonal flow U (green contours), and the low-level (850 hPa) tracks of cyclones (blue lines) and anticyclones (red lines), based on ERAI reanalysis data, for (a) 00:00 UTC Dec 7th, and (b) 18:00 UTC Dec 11th. The blue (red) dots denote the location of the cyclones (anticyclones) at the moment of the breaking, while the triangles denote the origin of the track. The centeroid of the AWB (CWB) is denoted by a star (diamond), and the black line denotes the 2.5 (5.5) PVU contour. The lowest contour of U is equal to 30 ms^{-1} and the contour spacing is 10 ms^{-1}. Panels (c) and (d) show the time-mean upper-level (250 hPa) zonal flow U (colors) together with the normalized Probability Density Functions (PDFs) (calculated using a kernel density estimator) of AWB and CWB centers, respectively, with lowest contour equal to 0.45 and contour intervals of 0.125.

https://doi.org/10.5194/egusphere-2023-534
Preprint. Discussion started: 23 March 2023
© Author(s) 2023. CC BY 4.0 License.

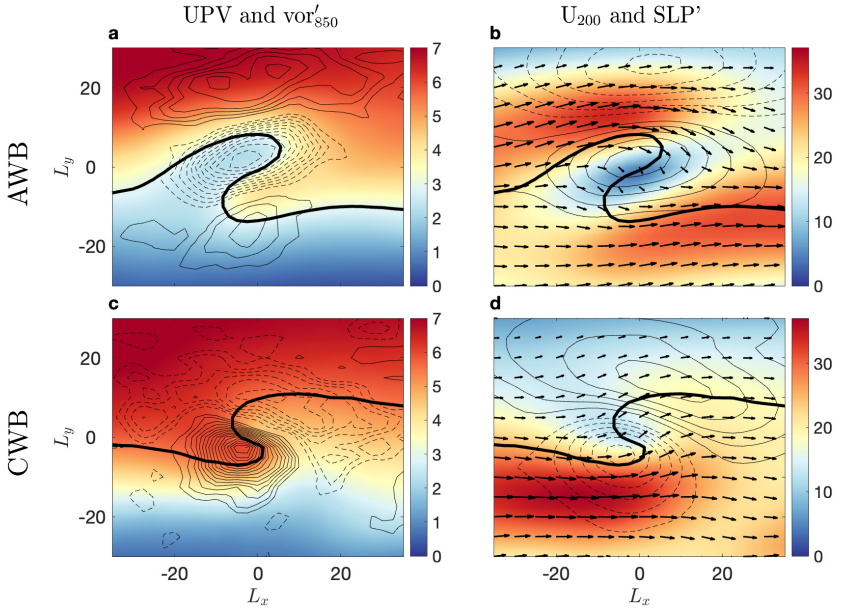

Figure 2. Composites of AWB (a,b) and CWB (c,d) events in the North-Atlantic region, based on ERA-Interim reanalysis data, which occurred over the years 1980-2014 during December-February (DJF). Panels (a),(c) show the upper-level (250 hPa) PV field (in PVU, colors) and the 850 hPa vorticity anomaly (in 10^{-5} s^{-1}, black contours), while panels (b),(d) show the upper-level (250 hPa) zonal flow (in ms^{-1}, colors) and the SLP anomaly (in mb, black contours), where the arrows denote the corresponding upper-level velocities. L_y and L_x denote the relative latitudinal and longitudinal distance (in degrees), respectively, from the center of the breaking. The black thick line in AWB (CWB) denotes the 2.5 (4.5) PVU contour. The lowest vorticity (SLP) anomaly contour is 0.15 (1), and the contour intervals are 0.1 (1).

https://doi.org/10.5194/egusphere-2023-534
Preprint. Discussion started: 23 March 2023
© Author(s) 2023. CC BY 4.0 License.

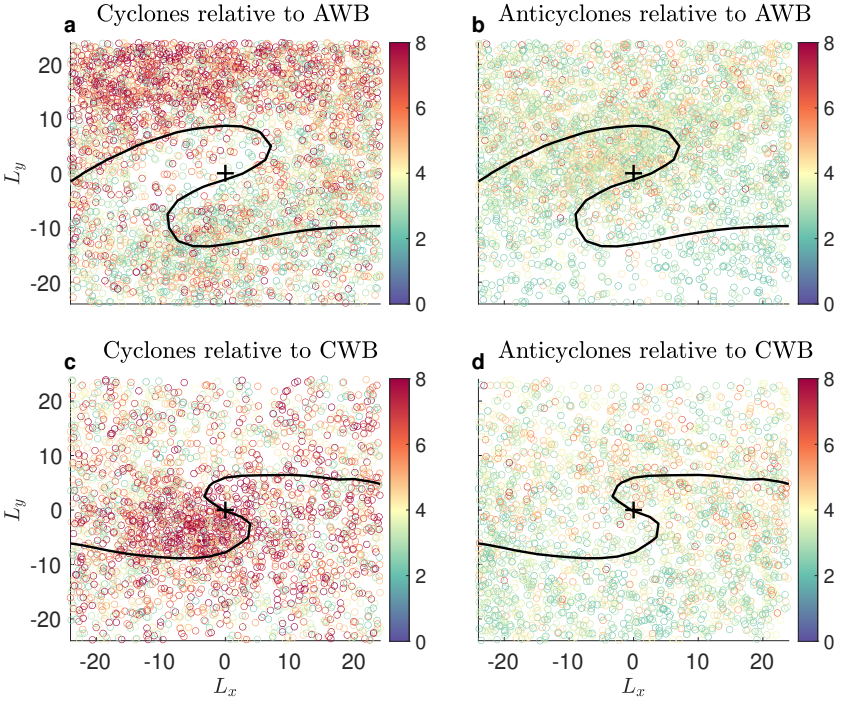

Figure 3. The positions of cyclones (a,c) and anticyclones (b,d) during AWB (first row) and CWB (second row), relative to the center of the RWB event (given by the cross symbol). Color indicates the intensity of the system, as identified by the tracking algorithm, in units of $10^{-5}\mathrm{s}^{-1}$, and only systems with intensities larger than $2 \cdot 10^{-5}\mathrm{s}^{-1}$ are plotted. L_y and L_x denote the relative latitudinal and longitudinal distance (in degrees), respectively, from the center of the breaking. The black thick line in the composites of AWB (CWB) denotes the 3 (5) PVU contour.

https://doi.org/10.5194/egusphere-2023-534
Preprint. Discussion started: 23 March 2023
© Author(s) 2023. CC BY 4.0 License.

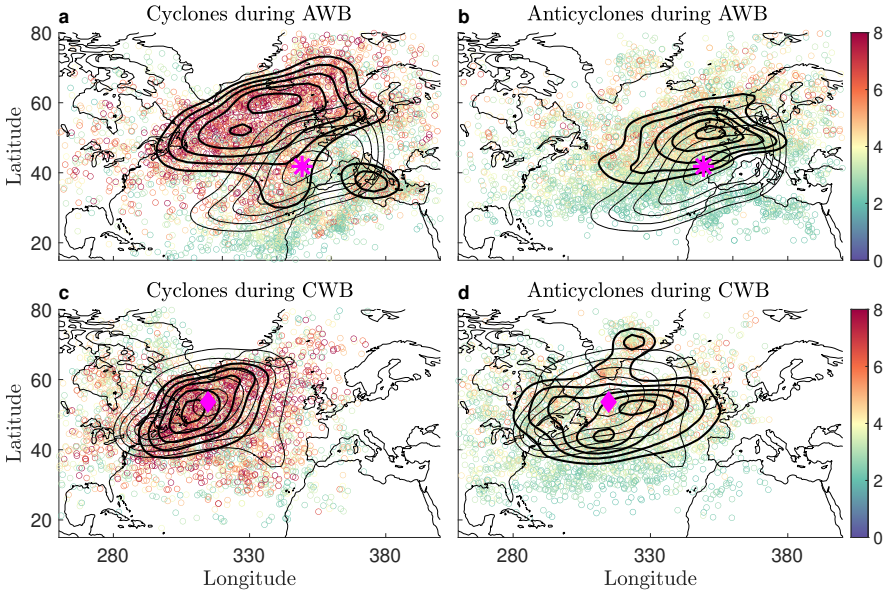

Figure 4. The actual spatial locations of cyclones (a,c) and anticyclones (b,d) during AWB (first row) and CWB (second row), where color indicates the intensity of the system in units of $10^{-5}\mathrm{s}^{-1}$, and only systems with intensities larger than $2 \cdot 10^{-5}\mathrm{s}^{-1}$ are plotted. Thick black contours are the normalized Probability Density Functions (PDFs) of the storm counts (calculated using a kernel density estimator), showing the locations where storms are most observed. The thin black contours show the normalized PDF of AWB (panels a,b, similar to Fig. 1c) and CWB westward of 350° (panels c,d, similar to Fig. 1d, except there the center east of 350° is shown as well), and the magenta star (diamond) denote the location where AWB (CWB) centroids are most frequently found. For all PDFs, the lowest contour is equal to 0.45 and the contour intervals are 0.125.

https://doi.org/10.5194/egusphere-2023-534
Preprint. Discussion started: 23 March 2023
© Author(s) 2023. CC BY 4.0 License.

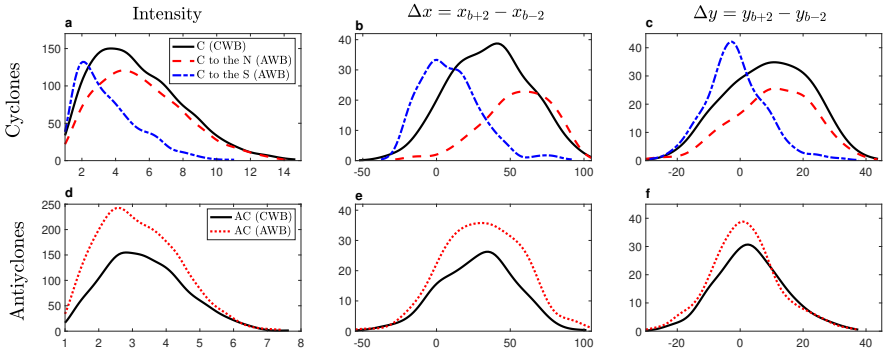

Figure 5. Fitted histogram lines, showing the distribution of the intensity (a,d), longitudinal displacements (b,e) and latitudinal displacements (c,f) of cyclones (first row) and anticyclones (second row) during RWB events. For cyclones, these are separated into cyclones during CWB (solid black lines), cyclones found more than 5° to the north (N) of AWB (red dashed lines), and cyclones found more than the 5° to the south (S) of AWB (dotted dashed blue lines). For anticyclones, the separation is only between anticyclones during CWB (solid black lines) and anticyclones during AWB (dotted red lines). Overall, there are 3,176 (4,960) anticyclones and 5,000 (3,372) cyclones found during AWB (CWB), where 2,704 cyclones are found 5° to the north and 2,296 cyclones are found 5° to the south of the AWB centroid. The displacements are calculated as the difference between the position two days after the breaking, minus the position two days prior to the breaking, so only cyclones and anticyclones lasting for more than 5 days are used in this case. Hence, for panels (b),(c),(e) and (f), only 708 (534) anticyclones and 1,198 (821) cyclones are used for AWB (CWB), where 568 cyclones reside 5° to the north and 630 cyclones reside 5° to the south of the AWB centroid. Similar results are found for displacements calculated in different manners.

https://doi.org/10.5194/egusphere-2023-534
Preprint. Discussion started: 23 March 2023
© Author(s) 2023. CC BY 4.0 License.

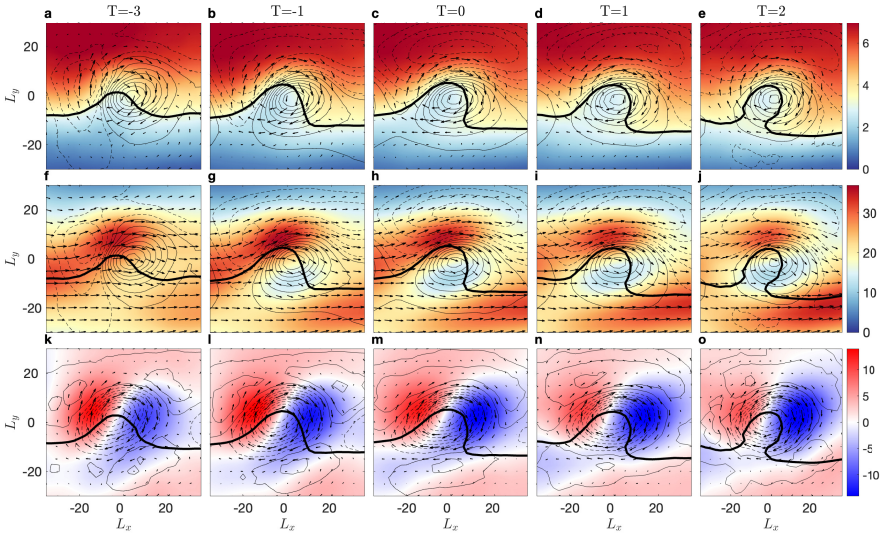

Figure 6. Composites centered around anticyclones during AWB events, showing the time evolution of AWB in the North-Atlantic region, from three days prior to the breaking ($T = -3$), and up to two days after the breaking ($T = 2$). Shown are the upper-level (250 hPa) PV in PVU (colors) and the SLP anomaly in mb (contours) (first row), the upper-level (250 hPa) zonal velocity in ms^{-1} (colors) and SLP anomaly in mb (contours) (second row), and the upper-level (250 hPa) meridional velocity in ms^{-1} (colors) and upper-level PV anomaly in PVU (contours) (third row). The arrows in panels (f-j) show the full upper-level velocities, while in panels (a-e) and (k-o) the anomalous upper-level velocities are shown. L_y and L_x denote the relative latitudinal and longitudinal distance (in degrees), respectively, from the center of the anticyclone. In all panels, the black line denotes the 3.2 PVU contour. The lowest contour for the SLP (PV) anomalies is 1 (0.1), while the contour interval is equal to 1 (0.2), where solid contours denote positive values and dashed contours denote negative values.

https://doi.org/10.5194/egusphere-2023-534
Preprint. Discussion started: 23 March 2023
© Author(s) 2023. CC BY 4.0 License.

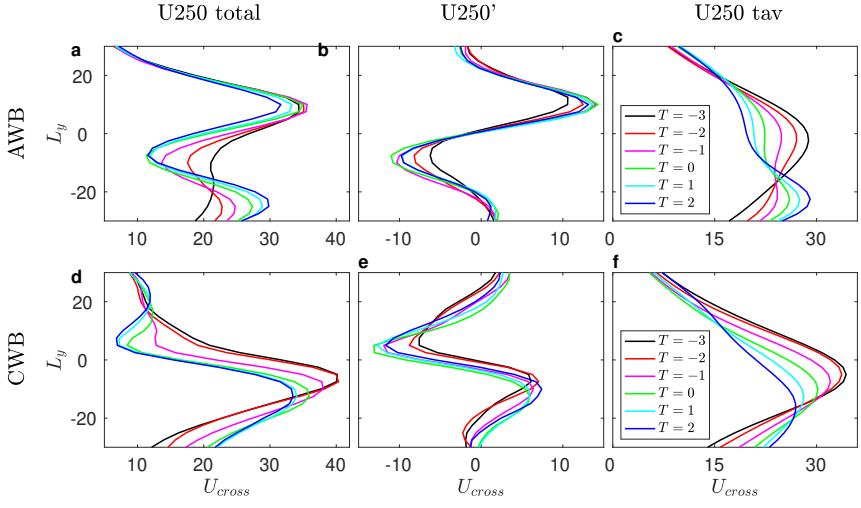

Figure 7. Cross sections of the composite upper-level (250 hPa) (a) total, (b) anomalous (deviation from time mean), and (c) climatological zonal velocity (in units of ms^{-1}), at the longitude crossing the center of the anticyclones during AWB events. Panels (d), (e) and (f) show the same fields, but for cyclones during CWB events. The colors indicate the time, going from black (three days prior to the breaking), to blue (two days after the breaking). L_y is the relative latitudinal distance (in degrees) from the center of the breaking.

https://doi.org/10.5194/egusphere-2023-534
Preprint. Discussion started: 23 March 2023
© Author(s) 2023. CC BY 4.0 License.

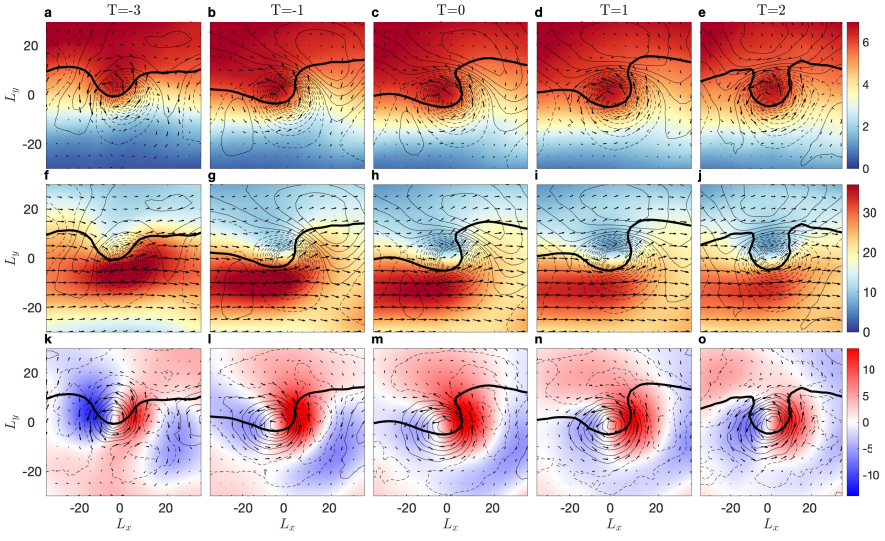

Figure 8. Same as Fig. 4, but for composites centered around cyclones during CWB events, showing the time evolution of CWB in the North-Atlantic region. In all panels, the black line denotes the 5.8 PVU contour.

https://doi.org/10.5194/egusphere-2023-534
Preprint. Discussion started: 23 March 2023
© Author(s) 2023. CC BY 4.0 License.

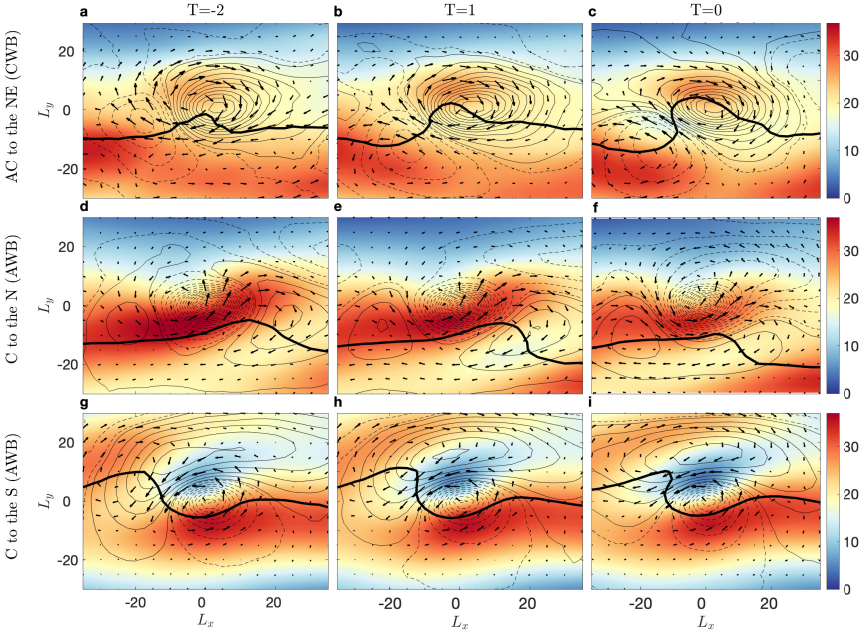

Figure 9. Anomalous life-cycles, showing composites centered around anticyclones residing to the northeast (NE) of the breaking center during CWB events (a-c), and around cyclones residing more than 5° to the north (N) (d-f) and more than 5° to the south (S) (g-i) of AWB in the North-Atlantic region, from one day prior to the breaking ($T = -1$), and up to one day after the breaking ($T = 1$). Shown are the upper-level (250 hPa) zonal velocity (colors) in ms^{-1} and the SLP anomaly in mb (contours), while the arrows denote the anomalous upper-level velocities. L_y and L_x denote the relative latitudinal and longitudinal distance (in degrees), respectively, from the center of the breaking. The black thick line denotes the 4.5 PVU contour in panels (a-c), the 3 PVU contour in panels (d-f), and the 3.5 PVU contour in panels (g-i).

https://doi.org/10.5194/egusphere-2023-534
Preprint. Discussion started: 23 March 2023
© Author(s) 2023. CC BY 4.0 License.

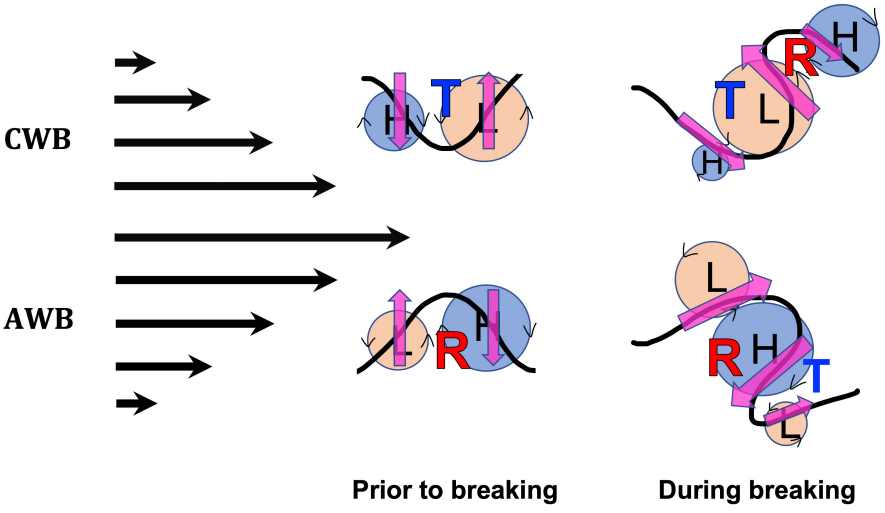

Figure 10. A schematic illustration showing the evolution of the upper- and lower-level flows during CWB (first row) and AWB (second row). The large black arrows on the left represent the background jet and the corresponding shear. The 'H' and 'L' symbols represent the low-level anticyclone (high-pressure anomaly) and cyclone (low-pressure anomaly), while the 'R' and 'T' symbols represent the upper-level ridge and trough, respectively. The pink arrows represent the anomalous upper level velocities, while the thin black arrows represent the anomalous low-level velocities. Note that the size of L and H represents the intensity of the system and not the size in physical space.